

Lattice wave emission from a moving dislocation

H. Koizumi

Department of Physics, Meiji University, Tama-ku, Kawasaki 214-8571, Japan

H. O. K. Kirchner

Institut de Sciences des Matériaux, Université Paris-Sud, Bâtiment 413, F-91405 Orsay, France

T. Suzuki

Institute of Industrial Science, University of Tokyo, Roppongi, Minato-ku, Tokyo 106-8558, Japan

(Received 3 August 2001; published 28 May 2002)

A dislocation moving in a lattice accelerates and decelerates due to the lattice periodicity and emits lattice waves. Simulations of this process in square and triangular lattices have been presented. Under a small stress, less than 70–80 % of the Peierls stress, a dislocation moving from an unstable position cannot overcome the next Peierls hill because it loses energy by emitting lattice waves. With a larger stress a long-distance motion of a dislocation is possible. When a dislocation moves slowly, lattice waves of dipolar type are emitted in the direction perpendicular to the motion of the dislocation. When the dislocation velocity is about half of the shear wave velocity, a V-shaped pattern of strong lattice vibration forms behind the moving dislocation because of the restricted propagation directions of the excited lattice waves. When the dislocation velocity exceeds 70% of the shear wave velocity, pair creation of dislocations occurs, which leads to dislocation cascading. A dislocation can move faster than the shear wave velocity in the square lattice, and there is no discontinuous change between subsonic and supersonic motions. The dislocation velocity is not proportional to the applied stress. The energy loss of the moving dislocation is about one order of magnitude larger than the theoretical value estimated by phonon-scattering mechanisms, even at room temperature.

DOI: 10.1103/PhysRevB.65.214104

PACS number(s): 61.72.Lk, 62.20.Fe, 63.20.Mt

I. INTRODUCTION

Dislocation motion is driven by external stress. At finite temperatures the thermal fluctuation of the crystal lattice triggers the motion (thermal activation). The moving dislocation loses energy by viscous drag due to phonon and/or electron scattering. It can also dissipate energy by radiating acoustic waves. Dynamical processes of dislocations, such as vibration, depinning from local obstacles, and kink pair formation for overcoming the Peierls potential, have been investigated by writing the equation of motion of a dislocation in an appropriate approximation, for example, the string model. In the equation of motion, only the viscous drag proportional to the dislocation velocity has been taken into account, but the radiation loss so far has been ignored. The equation of Granato and Lüke¹ for amplitude-independent internal friction has been used to determine the coefficient of viscosity.² The equation was modified by adding a term due to the Peierls potential and was used to simulate the motion of a dislocation on the Peierls relief.^{3–5} The string model of a dislocation was also applied to the tunneling process of a dislocation through the Peierls potential.⁶ The viscous drag has been taken into account to explain low-temperature anomalies of plasticity as well.^{7–9} The difference of the flow stress of superconducting and normal states of superconducting metals is explained by assuming that the superconducting electrons do not contribute to the viscous drag.¹⁰

However, theories of this type, which ignore the radiation loss of a moving dislocation, are unsatisfactory due to the following reasons.

(1) In a simulation of dislocation motion on the Peierls

relief it was found that, even if the viscous drag due to electrons is taken into account, a dislocation forms multikink pairs, and, therefore, long-range motion is possible under a stress larger than 70% of the Peierls stress.⁵ This contradicts the experimentally obtained temperature dependence of the flow stress, because the flow stress of bcc metals¹¹ and of alkali halides of NaCl type¹² increases at least up to 95% of the Peierls stress with decreasing temperature.

(2) In insulating materials such as CsI and CsBr there are no free electrons, and the phonon contribution vanishes at 0 K. However, the flow stress of CsI and CsBr at 0 K is larger than the value theoretically expected.⁹ These facts suggest that the energy loss of moving dislocations is much larger than that due to viscous drag only.

It has been known from elasticity theory^{13–18} that when a dislocation accelerates, it emits lattice waves and loses kinetic energy. A rough estimate shows that radiation of lattice waves from a moving dislocation is large enough to explain the flow stress of CsBr at 0 K.¹⁹ In real materials, accelerating motion of a dislocation occurs when the dislocation surmounts point obstacles or when the dislocation vibrates between pinning points under cyclic stresses. Even when there are no extrinsic obstacles, the dislocation accelerates and decelerates owing to the lattice periodicity (the Peierls potential), and dissipates energy by emitting lattice waves. This intrinsic process is especially important in materials with large Peierls stress.

Wave emission from a dislocation moving on the Peierls relief was calculated by Al'shitz *et al.*²⁰ in the framework of the elasticity theory. For a dislocation in a discrete lattice, Celli and Flytzanis²¹ and Ishioka²² obtained analytically the

stress F necessary to maintain a steady motion of a dislocation as a function of the velocity v_d in a two-dimensional square lattice with a harmonic interatomic row potential. The stress has a minimum at one-half of the shear wave velocity, and when the dislocation velocity is less than one-third of the shear wave velocity, $F(v_d)$ diverges and changes discontinuously at several values of v_d . Although supersonic motion is impossible in the continuum, their calculations indicate that a dislocation can move with a velocity larger than the shear wave velocity c_t , and no discontinuity exists at $v_d = c_t$. The dislocation velocity is not a single-valued function of the applied stress. It is not clear whether a dislocation can move with a steady constant velocity or not.

Recently, Gumbsch and Gao^{23,24} made an atomistic simulation of an edge dislocation moving in a bcc lattice. They showed that it can move above the longitudinal wave velocity, between the longitudinal and transverse wave velocities, as well as below the transverse wave velocity, and that a discontinuity seems to exist between transonic and subsonic motion. In their figures, shock waves emitted from a fast moving dislocation are clearly visible. Because of their complicated geometry of an edge dislocation in a bcc lattice, both transverse and longitudinal waves are emitted and propagate in various directions. Physically it is necessary to understand much more: wavelength and frequency, propagation direction and amplitude, in short, the nature of the lattice waves emitted. A simulation on a simple model should be helpful to understand these aspects. For example, our work²⁵ on a screw dislocation in a square lattice identified dipolar waves excited by the forward motion, and quadrupolar waves excited by the breathing of the core of the dislocation. Gumbsch and Gao^{23,24} kept their dislocation at supersonic velocity, but the most interesting question is if and how the sound barrier can be broken. This requires continuous monitoring at all speeds. Wave emission depends on the lattice structure; a triangular lattice resembles the configurations in fcc, bcc, and hcp metals more than a square one.

Our aim is to solve the equations of motion of atomic rows in a dislocated crystal, to visualize the lattice waves emitted from the moving dislocation, at all velocities, from rest to the velocity of sound. To avoid the complexities arising from mode mixing, we treat a straight screw dislocation in square and triangular two-dimensional lattices, in which only shear waves are emitted and propagate.

II. CALCULATION

Figure 1 shows an x - y plane of a square and a triangular lattice, used in the present calculation. Each atomic row parallel to the z axis moves rigidly only in this direction. The distance between the atomic rows in the x - y plane is a in both lattices, and the distance between the lattice planes in the z direction is also a . Nearest-neighbor rows interact with a potential

$$U(\Delta u_{ij}) = \frac{Ga^2}{4\pi^2} \left(1 - \cos 2\pi \frac{\Delta u_{ij}}{a} \right) \quad (1)$$

in the square lattice or

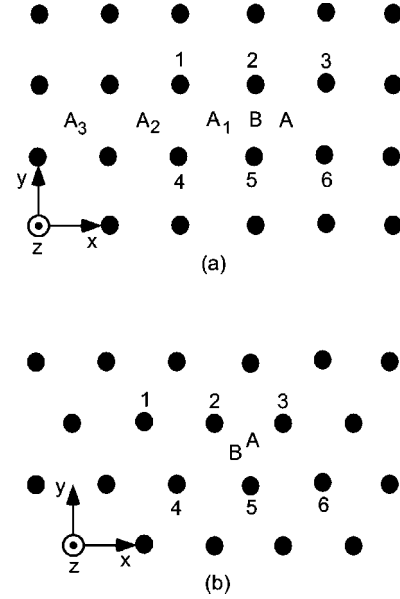


FIG. 1. A part of a square (a) and a triangular lattice (b). A is the stable equilibrium position and B is the unstable equilibrium position of a screw dislocation in the absence of applied stress ($F=0$).

$$U(\Delta u_{ij}) = \frac{Ga^2}{4\sqrt{3}\pi^2} \left(1 - \cos 2\pi \frac{\Delta u_{ij}}{a} \right) \quad (2)$$

in the triangular lattice, where G is the shear modulus and $\Delta u_{ij} = u_i - u_j$ is the difference of the displacements of the i th and j th atomic rows. Note that these potentials are different from the parabolic potential used by Celli and Flytzanis²¹ and by Ishioka.²² The lattice can be strained by applying forces in the z direction to the top and the bottom surfaces of the slab. The maximum stress that can be applied to the lattice or the ideal strength of the lattice F_{\max} is $G/2\pi$ and $G/\sqrt{3}\pi$ for the square and the triangular lattices, respectively. In the present model, the shear wave velocity c_t is the only characteristic velocity. For Cu and Si, c_t is 2.7×10^3 m/s and 6.2×10^3 m/s, and the time unit a/c_t is 9×10^{-14} s and 6×10^{-14} s, respectively. The mass of an atom is Ga^3/c_t^2 and $\sqrt{3}Ga^3/2c_t^2$ for the square and the triangular lattices, respectively.

A screw dislocation with the magnitude of the Burgers vector $b=a$ is introduced into the strained crystal. In the absence of applied force, the configuration A in Fig. 1 (the center of a square or of a triangle) is stable and the configuration B (the center of a bond) is the unstable equilibrium configuration. The stress at which no stable configuration can be found is the Peierls stress τ_p , and is $0.0159G$ and $0.0039G$, respectively, for the square and triangular lattices. For these lattices the difference of energy between the configurations B and A is $0.005066Ga^2$ and $0.000631Ga^2$ per atomic distance along the z direction, respectively.

A molecular-dynamics simulation is performed for 80×80 or 80×92 atomic rows, respectively, at zero absolute temperature, which means that there is initially no kinetic energy in the system. The initial configuration of the dislo-

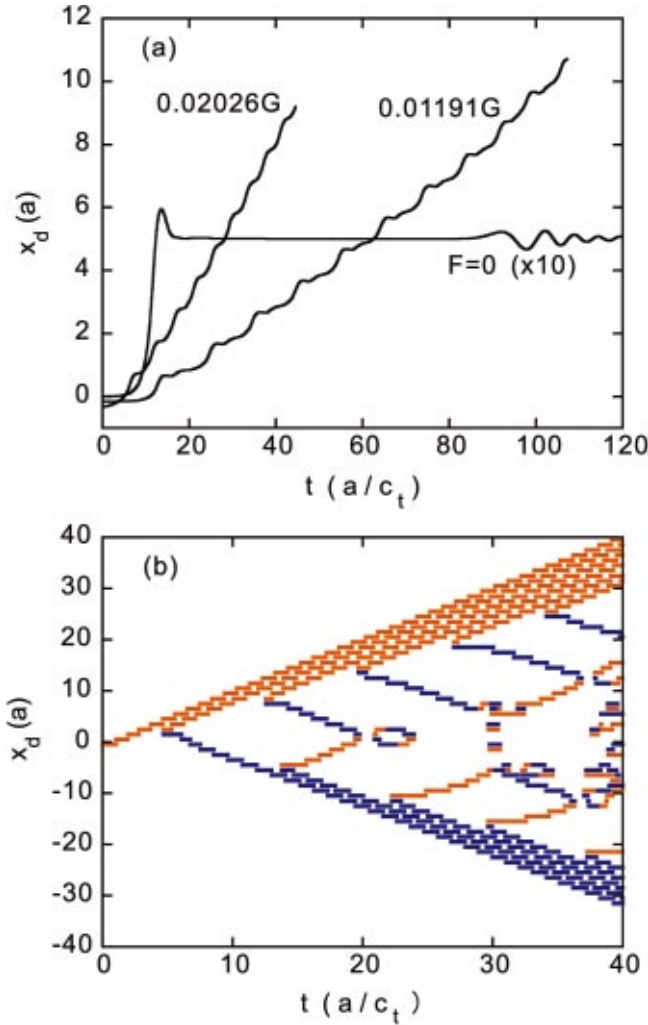


FIG. 2. (Color) Time dependence of the dislocation position x_d in the square lattice. The x coordinate of the position B is 0. (a) When the applied stress is zero, the dislocation moves to the position A ($x_d=0.5a$). When the applied stress $F=0.01191G$, the steady velocity of the dislocation v_d is $0.102c_t$, and when $F=0.02026G$, $v_d=0.251c_t$. (b) $F=0.1520G$ and $v_d=1.001c_t$. The orange and blue lines are the positions of positive and negative dislocations on the $y=0$ plane.

cated crystal is obtained by the following method when the applied force is smaller than the Peierls stress: (1) The displacement of the elastic solution for a dislocation (x_d, y_d) is imposed on the perfect lattice. (2) The lattice is relaxed under the condition that the relative displacement of the atomic rows (2 and 5) in the dislocation core is fixed. (3) If the residual forces on the atomic rows 2 and 5 after relaxation are zero, the configuration is the unstable equilibrium configuration under the applied stress. When the applied stress is larger than the Peierls stress, no unstable equilibrium configuration exists.

Starting from this initial position, the motion of the dislocation and the emission of the lattice waves are traced by integrating the equations of motion for all atomic rows in the crystal. Even when the dislocation is placed at an unstable equilibrium position under an applied stress less than the Peierls stress, it starts moving due to small residual forces.

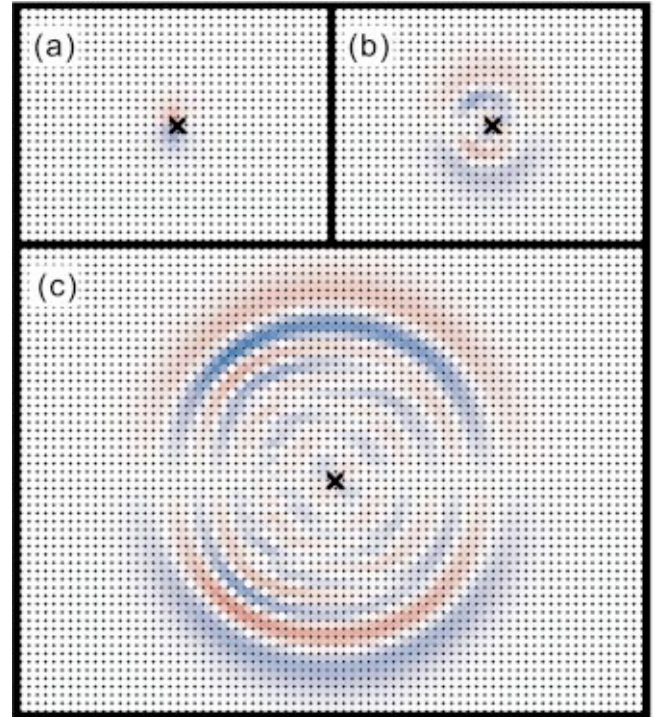


FIG. 3. (Color) Emitted waves from a moving dislocation at $F=0$. (a) $t=12.553a/c_t$, (b) $t=17.548a/c_t$, (c) $t=33.966a/c_t$. The direction of the motion of atomic row is shown by red and blue colors, and strong colors mean large velocities. The position of the dislocation is indicated with a cross. The maximum velocity v_{\max} of the atomic rows is $0.040c_t$, $0.0121c_t$, and $0.0046c_t$ in the cases (a), (b), and (c), respectively.

The dislocation position (x_d, y_d) is determined by

$$u_j = \frac{a}{2\pi} \tan^{-1} \frac{y_j - y_d}{x_j - x_d} \quad (3)$$

from the displacement $u_j(x_j, y_j)$ of the atomic rows near the dislocation (atomic rows 2, 3, 5, and 6 when the dislocation is near A and 1, 2, 3, 4, 5, and 6 when it is near B in the square lattice, and 2, 3, and 5 when the dislocation is near A and 2, 3, 4, and 5 when it is near B in the triangular lattice). In the case of the square lattice, y_d is always zero due to the symmetry of the lattice, but not in the triangular lattice, as described in the following section.

III. RESULTS

A. Square lattice

Even when the applied stress is zero, a dislocation placed initially at an unstable equilibrium position B moves to the nearest stable position A [Fig. 1(a)]. It stops at the stable position after some vibrating motion and does not move until the reflected waves from the surface reach the dislocation at the time of about $80a/c_t$ [Fig. 2(a)]. The emitted waves are shown in Fig. 3. The displacement u_i of each atomic row includes the contributions of the dislocation field and the emitted waves, and we have no *a priori* method to identify the two contributions separately. Therefore, in Fig. 3 the ve-

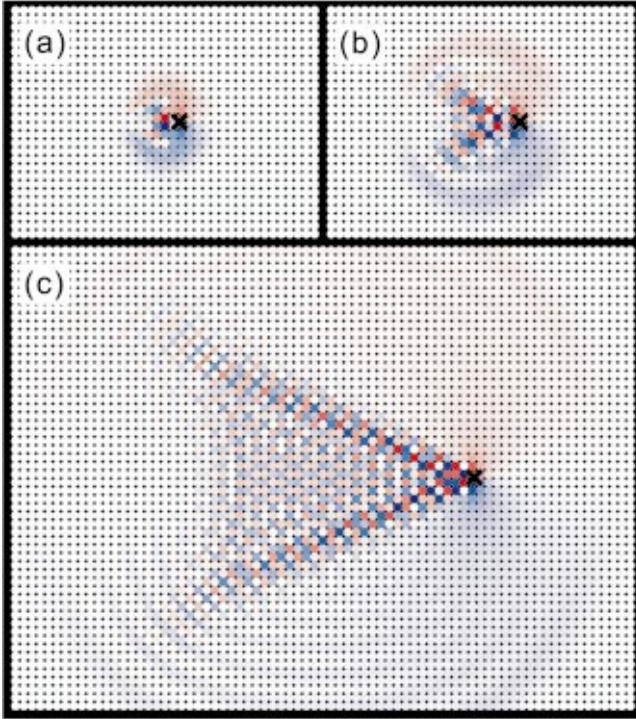


FIG. 4. (Color) Emitted waves from a moving dislocation with a velocity of $0.51c_t$ under the applied stress $F=0.051G$. (a) $t = 6.36a/c_t$, (b) $t = 6.95a/c_t$, (c) $t = 37.69a/c_t$. The meaning of the colors and the contrast are the same as in Fig. 3. The maximum velocity v_{\max} of the atomic rows is $0.125c_t$, $0.176c_t$, and $0.201c_t$ in the cases (a), (b), and (c), respectively. The position of the dislocation is indicated with a cross.

locity of each atomic row is shown with colors of contrasts proportional to the magnitude of the velocity. The color, red or blue, indicates the direction of the motion of the atomic row; forward or backward. The maximum velocity v_{\max} of atomic rows rapidly decreases with the time proceeding, so that the color contrasts of the three parts in Fig. 3 are not the same, but are adjusted to the observed maximum velocity v_{\max} as noted in the caption. The position of the dislocation is indicated with a cross. When a dislocation moves from B to A , it emits dipolar waves that are antisymmetric with respect to the slip plane [Fig. 3(a)]. It emits quadrupolar waves, anticentrosymmetric with respect to the dislocation position, when the dislocation is in the bottom of the Peierls potential [Figs. 3(b) and 3(c)]. Although the dislocation does not move, the quadrupolar waves continue to be emitted.

When the applied stress is larger than $0.73\tau_p$ or $0.0119G$, a dislocation repeats acceleration and deceleration (or even backward motion when the stress is relatively small) and continues motion, overcoming the Peierls relief [Fig. 2(a)]. The velocity averaged over one lattice distance becomes almost constant after the dislocation moves a few atomic distances. The dislocation continues steady motion before it encounters the lattice waves reflected at the surface. As the applied stress increases and the velocity of the dislocation becomes large, the modulation due to the Peierls relief becomes small. When a dislocation velocity is about half of the

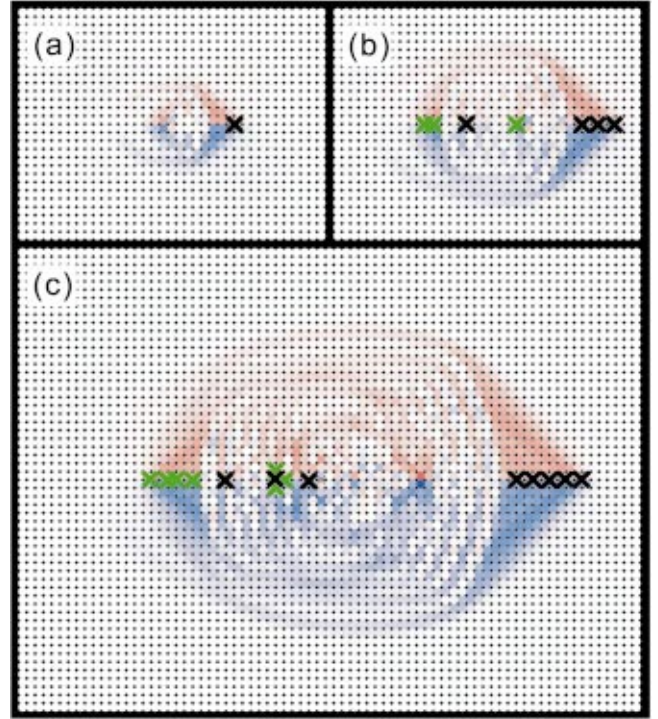


FIG. 5. (Color) Emitted waves from a moving dislocation with a velocity of $1.13c_t$ under the applied stress of $F=0.157G$. (a) $t = 7.65a/c_t$, (b) $t = 14.46a/c_t$, (c) $t = 28.28a/c_t$. The meaning of the colors and the contrast are the same as in Fig. 3. The maximum velocity v_{\max} of the atomic rows is $0.371c_t$, $0.331c_t$, and $0.448c_t$ in the cases (a), (b), and (c), respectively. The positions of the dislocations determined by the Burgers circuit method are indicated with black (positive dislocation) and green crosses (negative dislocation).

shear wave velocity, a V-shaped pattern of strong lattice vibration is observed behind the moving dislocation (Fig. 4).

When the dislocation moves faster than 70% of the shear wave velocity, dislocation pair creation occurs. In Fig. 5 black and green crosses indicate the positions of positive and negative dislocations, as determined by the Burgers circuit method. When the leading dislocation is at A in Fig. 1, pair creation occurs at the positions A_1 and A_2 or A_2 and A_3 . All dislocations are found within a distance a from the original slip plane. The positions of all dislocations on the original slip plane are shown in Fig. 2(b) as a function of time. The created positive dislocations move in the same direction as the leading dislocation, and the negative dislocations move in the opposite direction. The velocity of the daughter dislocations reaches the velocity of the mother dislocation after they move a few atomic distances.

The velocity v_d of this steady motion is plotted in Fig. 6 as a function of applied stress F . The $v_d(F)$ relation shows an abrupt change of slope at $v_d \approx 0.2c_t$. The dislocation velocity exceeds the shear wave velocity c_t when the applied stress is about 95% of the ideal crystal strength F_{\max} and there is no discontinuity at $v_d = c_t$.

B. Triangular lattice

Because the lattice is not symmetric with respect to the y plane, traces of a moving dislocation in the triangular lattice

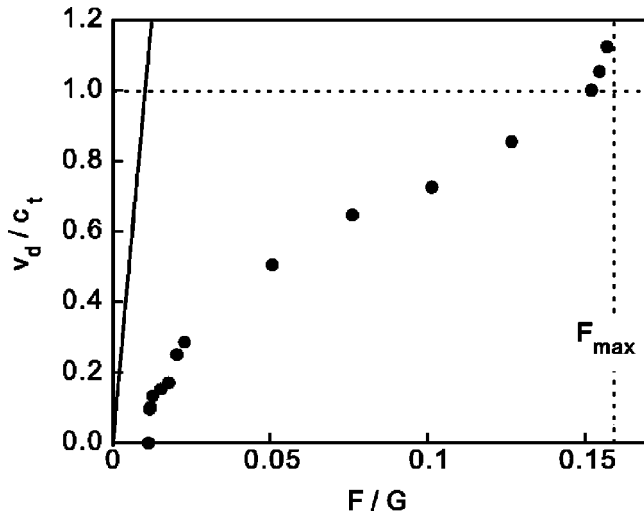


FIG. 6. The dislocation velocity v_d of the steady motion as a function of the applied stress F in the square lattice. The relation of Eq. (6) with $B=1 \times 10^{-2}Ga/c_t$ is shown by the oblique solid line.

are not straight but deviate from the x axis. Figure 7 shows the x and y coordinates of the dislocation position as a function of time t . When the stress is zero, a dislocation starting motion from an unstable equilibrium position B in Fig. 1(b) stops at the nearest stable position after a few vibrating motions (Fig. 7). It does not move until the reflected waves at the surfaces return to the dislocation position. The dislocation moves on the line shown in Fig. 8(d), and the emitted waves are of dipolar type. Figures 8(a) and 8(c) show the lattice waves when the dislocation moves to the right, and in Fig. 8(b) the lattice waves emitted from a dislocation moving to the left are shown. The polarity of the emitted waves is reversed when a dislocation moves in reverse.

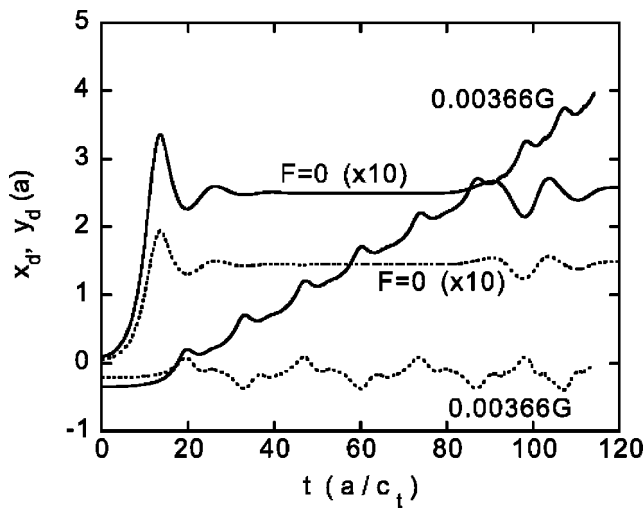


FIG. 7. Time dependence of dislocation position (x_d, y_d) in the triangular lattice. x_d is shown by solid lines and y_d by dotted lines. The x and y coordinates of the position B are 0. When the applied stress is zero, the dislocation moves to the position $A((x_d, y_d) = (a/4, \sqrt{3}a/12))$. When the applied stress $F=0.00366G$, the steady velocity of the dislocation v_d is $0.0373c_t$.

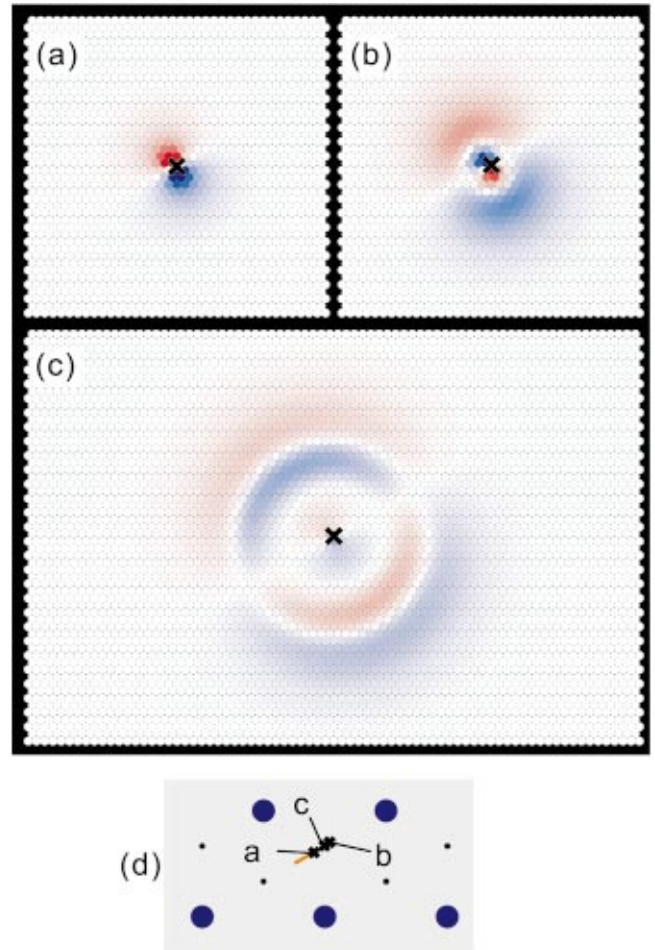


FIG. 8. (Color) Emitted waves from a moving dislocation at $F=0$. (a) $t=9.735a/c_t$, (b) $t=15.331a/c_t$, (c) $t=24.075a/c_t$. The meaning of the colors and the contrast are the same as in Fig. 3. The maximum velocity v_{\max} of the atomic rows is $0.01645c_t$, $0.00780c_t$, and $0.001920c_t$ in the cases (a), (b), and (c), respectively. The position of the dislocation is indicated with a cross. In (d) the trace of the dislocation movement is shown by the orange line, and the crosses marked with a, b, and c are the positions of the dislocation at three times (a), (b), and (c), respectively. The lattice points are indicated with blue circles and the stable positions of a dislocation with black dots.

When the stress is larger than $0.81\tau_p$ or $0.0032G$, a dislocation overcomes the Peierls potential and the long-distance motion occurs (Fig. 7). While the applied stress is not large, a dislocation moves keeping away from the lattice points [Fig. 9(e)], and takes a nonplanar zigzag path like a wiggler, in contrast with the planar path in the square lattice. Figures 9(a)–9(d) show the emitted waves when a dislocation is at the positions a – d shown in Fig. 9(e). The relation between the polarity of the emitted dipolar waves and the direction of the dislocation motion is always the same as in Fig. 8. When the dislocation velocity is about half of the shear wave velocity, the emitted waves form a V-shaped pattern of strong lattice vibrations behind the dislocation as shown in Fig. 10.

When the applied stress is larger than $0.15G$ and the velocity is larger than $0.8c_t$, pair creation of dislocations oc-

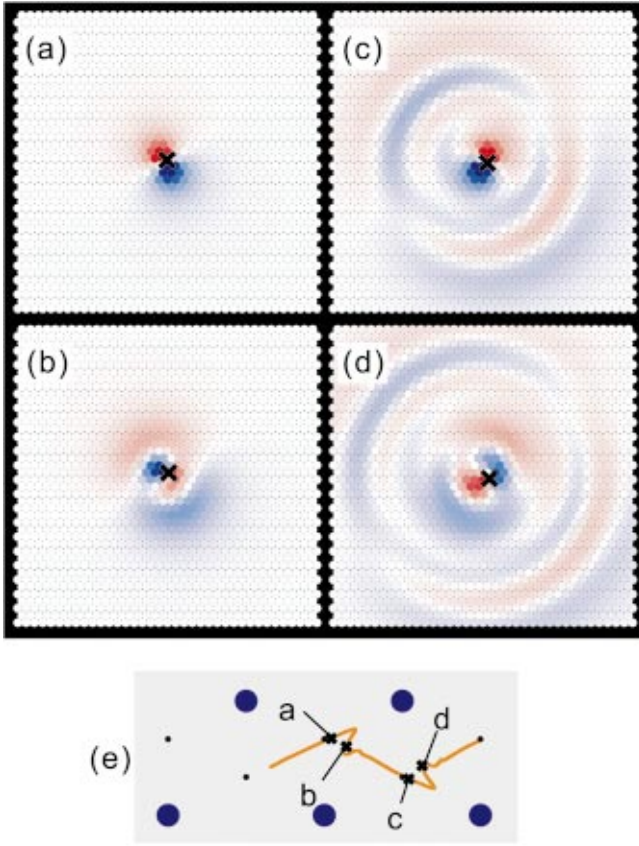


FIG. 9. (Color) Emitted waves from a moving dislocation with a velocity of $0.037c_t$ under the applied stress $F=0.003\,66G$. (a) $t=17.877a/c_t$, (b) $t=21.864a/c_t$, (c) $t=31.231a/c_t$, (d) $t=35.769a/c_t$. The meaning of the colors and the contrast are the same as in Fig. 3. The maximum velocity v_{\max} of the atomic rows is $0.031\,46c_t$, $0.014\,34c_t$, $0.033\,08c_t$, and $0.010\,35c_t$ in the cases (a), (b), (c), and (d), respectively. The position of the dislocation is indicated with a cross. In (e) the trace of the dislocation movement is shown by the orange line, and the crosses marked with a, b, c , and d are the positions of the dislocation at four times (a), (b), (c), and (d), respectively. The lattice points are indicated with blue circles and the stable positions of a dislocation with black dots.

curs in the triangular lattice, just as in the square lattice. The emitted waves and the positions of all the dislocations are shown in Fig. 11. In the triangular lattice, unlike in the square lattice, the pair creation does not always occur at the position next to the mother dislocation, but often occurs several atomic distances behind the mother dislocation. Furthermore, the created dislocations move not only in the x direction but also in the $[\pm 1, \sqrt{3}, 0]$ directions, while the leading dislocation moves on the $y=0$ plane. As a result, nucleated dislocations form a cloud, as seen in Fig. 11(c), and we cannot draw a picture like Fig. 2(b) for the created dislocations in the messy region. However, the leading dislocation moves at constant velocity.

The velocity of the dislocation is plotted as a function of the applied stress in Fig. 12. In this case a discontinuous change in the slope of $v_d(F)$ occurs at $t \approx 0.1c_t$. Unlike in the square lattice, the shear wave velocity is not attained.

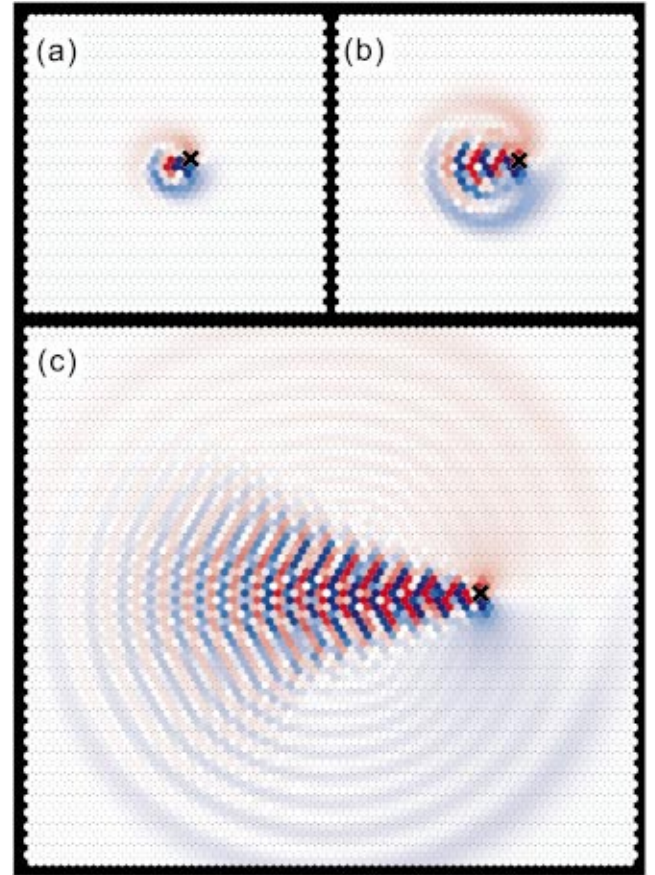


FIG. 10. (Color) Emitted waves from a moving dislocation with a velocity of $0.51c_t$ under the applied stress of $F=0.0731G$. (a) $t=6.900a/c_t$, (b) $t=11.208a/c_t$, (c) $t=40.117a/c_t$. The meaning of the colors and the contrast are the same as in Fig. 3. The maximum velocity v_{\max} of the atomic rows is $0.2180c_t$, $0.2239c_t$, and $0.2666c_t$ in the cases (a), (b), and (c), respectively. The position of the dislocation is indicated with a cross.

IV. DISCUSSION

The results can be summarized as follows.

(1) Below a certain value of the applied stress F , a dislocation cannot overcome the Peierls potential and no long-distance motion occurs.

(2) With increasing F , long-distance motion becomes possible (Figs. 6 and 12). From the computer simulation it is not clear whether there is a jump in $v_d(F)$ at this critical stress.

(3) With further increase of F , the velocity increases monotonically. However, there is at least one abrupt change in the slope of the $v_d(F)$ relation.

(4) When the dislocation velocity is about half of the shear wave velocity, a V-shaped pattern forms behind the moving dislocation.

(5) When v_d is 70–80% of the shear wave velocity, dislocation pair creation starts.

(6) In the square lattice, supersonic motion of a dislocation was confirmed, while in the triangular lattice it was not observed.

As shown by the present authors,²⁵ translational motion of a dislocation causes dipolar emission, while core expansion

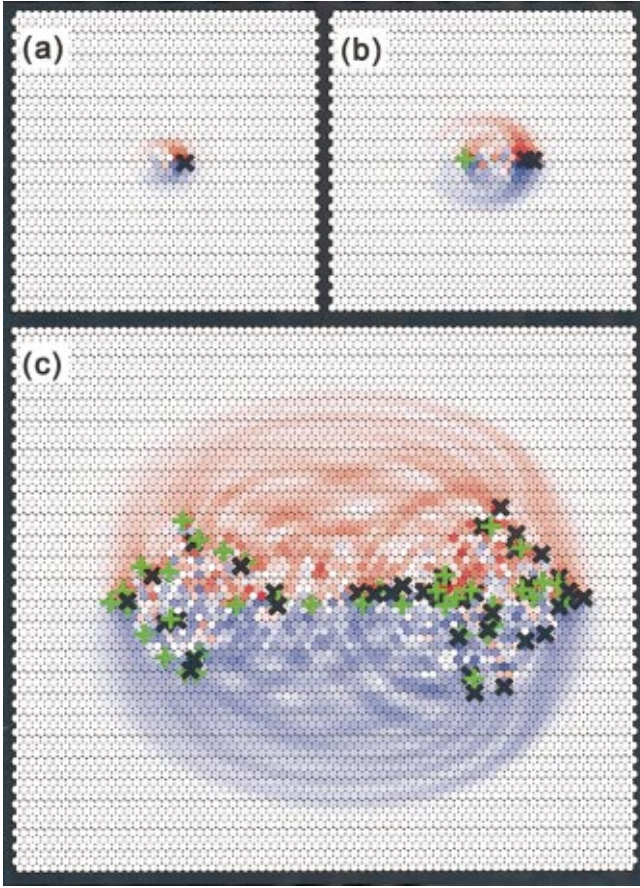


FIG. 11. (Color) Emitted waves from a moving dislocation with a velocity of $0.86c_t$ under the applied stress of $F=0.1755G$. (a) $t = 3.627a/c_t$, (b) $t = 7.803a/c_t$, (c) $t = 36.464a/c_t$. The meaning of the colors and the contrast are the same as in Fig. 3. The maximum velocity v_{\max} of the atomic rows is $0.3772c_t$, $0.3810c_t$, and $0.5408c_t$ in the cases (a), (b), and (c), respectively. The positions of the dislocations determined by the Burgers circuit method are indicated with black (positive dislocation) and green crosses (negative dislocation).

and shrinkage cause quadrupolar emission. Figures 3(a) and 8 correspond to the former case, and Figs. 3(b) and 3(c) to the latter. In addition, Fig. 9 for the triangular lattice shows that when the dislocation changes its direction of motion it always emits dipolar waves directed perpendicular to the dislocation motion. On the other hand, quadrupolar waves are not emitted in the triangular lattice, probably because of the threefold symmetry of the lattice.

For their harmonic models, Celli and Flytzanis²¹ and Ishioka²² showed that when a dislocation moves with a uniform velocity \mathbf{v}_d , the emitted waves satisfy $\omega = \mathbf{k} \cdot \mathbf{v}_d$, where \mathbf{k} is the wave vector and ω is the angular frequency of the excited waves.²⁶ The dispersion relation of phonons is

$$\omega(k_x, k_y) = \frac{2c_t}{a} \left(\sin^2 \frac{k_x a}{2} + \sin^2 \frac{k_y a}{2} \right)^{1/2} \quad (4)$$

in the square lattice and

$$\omega(k_x, k_y) = \frac{2\sqrt{2}c_t}{\sqrt{3}a} \left[\sin^2 \frac{k_x a}{2} + \sin^2 \frac{(k_x + \sqrt{3}k_y)a}{4} + \sin^2 \frac{(k_x - \sqrt{3}k_y)a}{4} \right]^{1/2} \quad (5)$$

in the triangular lattice. In Figs. 13 and 14 the intersection of $\omega(\mathbf{k})$ and $\omega = \mathbf{k} \cdot \mathbf{v}_d$, as well as $\omega(k_x, 0)$, are shown in the extended zone for both lattices. At $v_d \approx 0.217c_t$ for the square lattice and at $v_d \approx 0.138c_t$ for the triangular lattice, $\omega = \mathbf{k} \cdot \mathbf{v}_d$ is in contact with the dispersion relation. The abrupt changes in the slope of calculated $v_d(F)$ relations (Figs. 6 and 12) seem to occur around the v_d values obtained for a harmonic lattice, being attributed to the van Hove singularity.

The V-shaped patterns formed behind the dislocations at $v_d = 0.5c_t$ (Figs. 4 and 10) look like Cherenkov cones, but this is not true. Their interpretation is as follows: According to the selection rule $\omega = \mathbf{k} \cdot \mathbf{v}_d$ of wave emission,^{21,22} the wave vector \mathbf{k} of the emitted wave is given by the dot-dashed lines in Figs. 13(a) and 14(a). Since it belongs to the second and is close to the first Brillouin zone, the wave propagates backward from the moving dislocation. The group velocity of the wave is $(v_{gx}, v_{gy}) = (\partial\omega/\partial k_x, \partial\omega/\partial k_y)$ and, therefore, the direction angle ranges only between -48° and $+48^\circ$ from the $-x$ axis for the square lattice. Since the dislocation moves with the velocity $(v_d, 0)$, the successively emitted waves with the same \mathbf{k} vector form a line with an angle $\theta = \tan^{-1}[v_{gy}/(v_d - v_{gx})]$ from the $-x$ direction, as shown in Fig. 15. The lines for all possible \mathbf{k} vectors are superimposed to produce a triangular region of large amplitude. The front edges of the triangle are given by the largest and the smallest values of θ . As calculated from the dispersion relations, Eqs. (4) and (5), the maximum value of $|\theta|$ is 27° and 23° for the square and the triangular lattices, respectively. The angles of the V-shaped patterns in Figs. 4 and 10 agree well with these calculated values. Therefore, the appearance of the V-shaped

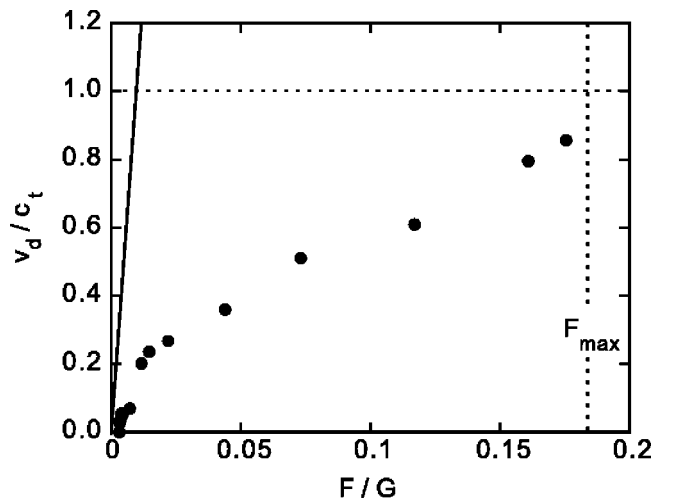


FIG. 12. The dislocation velocity v_d of the steady motion as a function of the applied stress F in the triangular lattice. The relation of Eq. (6) with $B = 1 \times 10^{-2}Ga/c_t$ is shown by the oblique solid line.

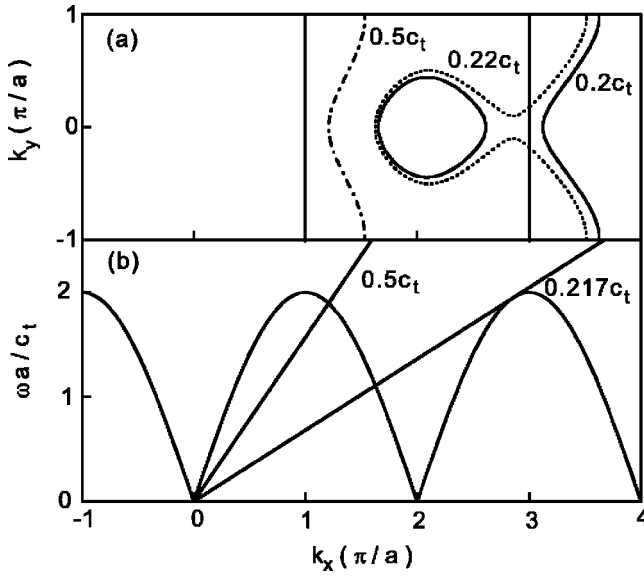


FIG. 13. (a) Wave vector \mathbf{k} that satisfies $\omega(k_x, k_y) = \mathbf{k} \cdot \mathbf{v}_d$ and (b) phonon-dispersion curve along the axis $k_y = 0$, $\omega(k_x, 0)$ for the square lattice.

patterns at subsonic velocity is just due to the strong anisotropy of the direction of wave emission. On the other hand, the wave fronts seen at trans/supersonic velocity (Figs. 5 and 11) should be Cherenkov cones.

As is shown in Figs. 5 and 11 a dislocation moving faster than $0.7c_t$ in the square lattice or $0.8c_t$ in the triangular lattice creates dislocation pairs. The possibility of pair creation near a fast moving dislocation was predicted by Ishioka²⁷ and confirmed by Schiotz and Jacobsen²⁸ by computer simulation. Ishioka suggested that pair creation occurs on a slip plane next to the original slip plane of a fast moving dislocation. However, the present simulation shows that in the square lattice, pair creation mostly occurs on the original slip plane.

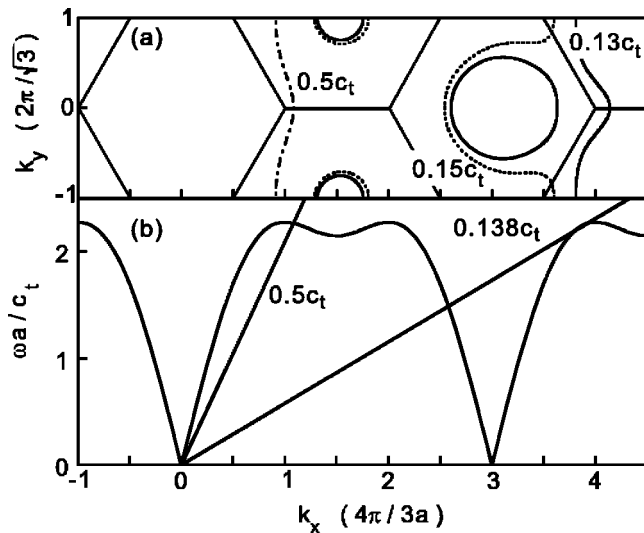


FIG. 14. (a) Wave vector \mathbf{k} that satisfies $\omega(k_x, k_y) = \mathbf{k} \cdot \mathbf{v}_d$ and (b) phonon-dispersion curve along the axis $k_y = 0$, $\omega(k_x, 0)$ for the triangular lattice.

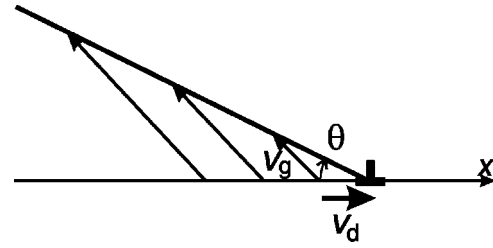


FIG. 15. A dislocation moving with velocity \mathbf{v}_d emits lattice waves that propagate with group velocity \mathbf{v}_g . The successively emitted waves with a certain \mathbf{k} vector leave a line behind the dislocation. The angle between the line and the $-x$ direction is $\theta = \tan^{-1}[v_{gy}/(v_d - v_{gx})]$.

Repeated pair creation of dislocations leads to dislocation cascading. In the square lattice, geometrically, dislocations can move either in the x or y direction, but under the applied shear force parallel to the x direction, dislocations move preferably in the $\pm x$ directions. This results in the cascade formation on the (010) slip plane, as seen in Figs. 2(b) and 5. On the contrary, in the triangular lattice, the created dislocation can glide not only in $[100]$ but also in $[\pm 1, \sqrt{3}, 0]$ directions, therefore, the dislocation cloud forms behind the leading dislocation, as seen in Fig. 11. In the cloud, pair creation and annihilation occur more frequently than in the square lattice.

Supersonic dislocation movement is not expected in the continuum elasticity theory. However, it is acceptable in the harmonic lattice theory.^{21,22} Supersonic motion has been demonstrated by Gumbsch and Gao^{23,24} in their computer simulation of an edge dislocation in a bcc lattice. In the present calculation, supersonic movement is confirmed in the square lattice, and there is no discontinuity in the $v_d(F)$ relation at $v_d = c_t$. If in Fig. 12, for the triangular lattice, the applied force F were taken much closer to the ideal strength F_{\max} , the dislocation velocity v_d might overcome the shear wave velocity c_t . However, confirmation of the supersonic motion is not important, because it is already found in the square lattice. To be noted here is the fact that the easiness of supersonic motion depends on the efficiency of energy dissipation. Since energy dissipation occurs not only on acceleration but also on turning the direction of motion, nonplanar or zigzag (wigglerlike) motion of a dislocation in the triangular lattice (Fig. 9) produces larger energy losses than the planar motion in the square lattice. This accounts for the result that the v_d - F curve for the triangular lattice (Fig. 12) is 20–30% lower than that for the square lattice (Fig. 6), and at the same time accounts for the hardness of supersonic motion in the triangular lattice.

Theories for dynamical processes of dislocations, which are usually based on the string model of a dislocation, have so far ignored the radiation loss, and exclusively considered the viscous drag due to free electrons and/or phonons, which is expressed as

$$Bv_d = Fa, \quad (6)$$

where B is the viscous drag coefficient. For Cu, experimentally obtained values of B fall in the range (1.2–6.5)

$\times 10^{-5}$ Pa s at room temperature^{2,29,30} or $(0.4-2) \times 10^{-2} Ga/c_t$, which is in rough agreement with theoretical estimates of phonon scattering by the lattice anharmonic strain field and the flutter effect.¹⁸ The electron-scattering contribution to B is smaller and is $2 \times 10^{-3} Ga/c_t$ for Pb.³¹ Above the Debye temperature the viscosity due to dislocation fluttering is $B \approx k_B T \omega_D^2 / \pi^2 c_t^3$, where ω_D is the Debye frequency, k_B is the Boltzmann constant, and T is the temperature.³² With $\omega_D \approx c_t(\pi/a)$, $B \approx (k_B T / Ga^3)(Ga/c_t)$. For most materials, $Ga^3 \approx 1$ eV, and, therefore, $B \approx 1/40(Ga/c_t)$ at room temperature. The oblique solid line in Figs. 6 and 12 is the relation of Eq. (6) with $B = 1 \times 10^{-2} Ga/c_t$. It is obvious that the drag force due to radiation loss can never be approximated by a linear relation such as Eq. (6), in particular, at low stresses. There is a certain threshold of F for the steady motion of a dislocation. As an overall trend, the radiation drag is about one order of mag-

nitude larger than the commonly accepted values of the phonon drag at room temperature. It should be noted that the experimental values of the drag coefficient found in the literatures^{2,29,30} have been derived simply by assuming Eq. (6) in the theory of Granato and Lücke¹ for internal friction without considering radiation loss. If the radiation loss in internal friction were reasonably taken into account, very different estimates of the viscous drag coefficient as well as other parameters of the theory would be obtained. The present results strongly suggest that in every theory concerning dynamical processes of dislocations, such as the underdamped unzipping process as a cause of the anomalous temperature dependence of the yield stress of fcc metals^{7,10} and ionic crystals of CsCl type^{8,9} at low temperatures, the kink pair formation process due to inertial effect,⁵ and also the tunneling process overcoming the Peierls potential,⁶ the radiation loss must be properly taken into account.

-
- ¹A. Granato and K. Lücke, *J. Appl. Phys.* **27**, 583 (1956).
²R.M. Stern and A.V. Granato, *Acta Metall.* **10**, 358 (1962).
³K. Sato and A. Sugiyama, *J. Phys. Soc. Jpn.* **40**, 1698 (1976).
⁴K. Sato and A. Sugiyama, *J. Phys. Soc. Jpn.* **47**, 889 (1979).
⁵T. Suzuki and H. Koizumi, *Philos. Mag. A* **67**, 1153 (1993).
⁶B.V. Petukov, H. Koizumi, and T. Suzuki, *Philos. Mag. A* **77**, 1041 (1998).
⁷For a review, T.A. Parkhomenko and V.V. Pustovalov, *Phys. Status Solidi A* **74**, 11 (1982).
⁸T. Suzuki and H. Koizumi, *Phys. Status Solidi A* **74**, K101 (1982).
⁹H. Koizumi and T. Suzuki, *Phys. Status Solidi A* **75**, 301 (1983).
¹⁰For a review, F.R.N. Nabarro and A.T. Quintanilha, in *Dislocations in Solids*, edited by F.R.N. Nabarro (North-Holland, Amsterdam, 1980), Vol. 5, p. 193.
¹¹T. Suzuki, Y. Kamimura, and H.O.K. Kirchner, *Philos. Mag. A* **79**, 1629 (1999).
¹²T. Suzuki and H. Koizumi, in *Proceedings of the International Symposium on Lattice Defect Related Properties of Dielectric Materials, Turawa, 1985*, edited by B. Macalik (Polish Academy of Science, Wrocław, 1986), p. 117.
¹³G. Leibfried, *Z. Phys.* **127**, 344 (1950).
¹⁴F.R.N. Nabarro, *Philos. Mag.* **42**, 1224 (1957).
¹⁵J.D. Eshelby, *Proc. R. Soc. London, Ser. A* **266**, 222 (1962).
¹⁶A. Ookawa and K. Yazu, *J. Phys. Soc. Jpn.* **18**, Suppl. 1, 36 (1963).
¹⁷J. Weertman and J. R. Weertman, in *Dislocations in Solids* (Ref. 10), Vol. 3, p. 1.
¹⁸J.P. Hirth and J. Lothe, *Theory of Dislocations*, 2nd ed. (Wiley, New York, 1982).
¹⁹H. Koizumi and T. Suzuki, in *Dislocations in Solids*, edited by H. Suzuki, T. Ninomiya, K. Sumino and S. Takeuchi (University of Tokyo Press, Tokyo, 1985), p. 479.
²⁰V.I. Al'shitz, V.L. Indenbom and A.A. Shol'tberg, *Zh. Eksp. Teor. Fiz.* **60**, 2308 (1971) [*Sov. Phys. JETP* **33**, 1240 (1971)].
²¹V. Celli and N. Flytzanis, *J. Appl. Phys.* **41**, 4443 (1970).
²²S. Ishioka, *J. Phys. Soc. Jpn.* **30**, 323 (1971).
²³P. Gumbsch and H. Gao, *Science* **283**, 965 (1999).
²⁴P. Gumbsch and H. Gao, *J. Comput.-Aided Mater. Des.* **6**, 137 (1999).
²⁵H. Koizumi, H.O.K. Kirchner and T. Suzuki, *Mater. Sci. Eng., A* **309-310**, 117 (2001).
²⁶Although Celli and Flytzanis (Ref. 21) and Ishioka (Ref. 22) obtained this relation for a harmonic lattice with nearest-neighbor interaction, it is a universal relation. When a dislocation moves at constant average velocity \mathbf{v}_d , it emits the same mode of the lattice wave at equivalent positions (for example, at the positions A , A_1 and A_2 in Fig. 1). If a wave emitted from the dislocation at $(0,0)$ is $\exp i(\mathbf{k} \cdot \mathbf{r} - \omega t)$, after the time t_0 , which satisfies $\mathbf{v}_d t_0 = \mathbf{a}$, \mathbf{a} being the lattice periodic vector parallel to \mathbf{v}_d , the wave emitted at position \mathbf{a} is $\exp i[(\mathbf{k} \cdot (\mathbf{r} - \mathbf{a}) - \omega(t - t_0))]$. The condition of constructive interference at $|\mathbf{r}| \gg |\mathbf{a}|$ is $\exp[i(-\mathbf{k} \cdot \mathbf{a} + \omega t_0)] = 1$, that is, $\omega = \mathbf{k} \cdot \mathbf{v}_d$.
²⁷S. Ishioka, *J. Phys. Chem. Solids* **36**, 427 (1975).
²⁸J. Schiotz and K.W. Jacobsen, *Philos. Mag. Lett.* **72**, 245 (1995).
²⁹T. Suzuki, A. Ikushima and M. Aoki, *Acta Metall.* **12**, 1231 (1964).
³⁰W.P. Mason and A. Rosenberg, *Phys. Rev.* **151**, 434 (1966).
³¹A. Hikata and C. Elbaum, *Phys. Rev. Lett.* **18**, 750 (1967).
³²T. Ninomiya, *J. Phys. Soc. Jpn.* **36**, 399 (1974).